Se intercalation between $PtSe_2$ and the Pt surface during synthesis of $PtSe_2$ by direct selenization of Pt(111)

Mihovil Bosnar,[1,*] Vasile Caciuc,[2] Nicolae Atodiresei,[2,†] Ivor Lončarić,[1] and Stefan Blügel[2]
[1]*Ruđer Bošković Institute, 10000 Zagreb, Croatia*
[2]*Peter Grünberg Institut (PGI-1) and Institute for Advanced Simulation (IAS-1), Forschungszentrum Jülich and JARA, D-52425 Jülich, Germany*

(Received 7 August 2020; accepted 25 August 2020; published 22 September 2020)

Using the first principles calculations, we analyze the structural and electronic properties of a $PtSe_2$ monolayer on Pt substrate, obtained by direct selenization of the Pt(111) surface [Wang *et al.*, Nano Lett. **15**, 4013 (2015)]. We demonstrate that in order to reproduce the experimental result that $PtSe_2$ is physisorbed on the surface, the surface must be passivated. We propose that this passivation is most likely due to intercalation of Se atoms between $PtSe_2$ and Pt surface during the selenization process. In this case the mean distance between the Se-passivated surface and $PtSe_2$ is found to be 3.24 Å, which is consistent with the distance that can be extracted from the scanning transmission electron microscopy image of the hybrid system, and the adsorption energy is found to fall into physisorption range. Therefore, our findings provide an insight into the synthesis of $PtSe_2$ by direct selenization: A realistic structural model should include a Se-passivated surface and not a clean one.

DOI: 10.1103/PhysRevB.102.115427

I. INTRODUCTION

Exfoliation of a stable monolayer from graphite in 2004 [1] demonstrated that it is possible to make atomically thin materials, which are essentially two-dimensional (2D) in nature. Since then, the interest in the fundamental properties and the potential applications of 2D materials has grown rapidly, and a number of them have been synthesized and characterized. Their distinctive geometry and electronic structure often provide interesting opportunities for development in various fields of application, such as photocatalysis [2], optoelectronics [2–8], thermoelectric devices [9], semiconductor electronics [1,8,10–12], and battery electrodes [13].

A vast majority of the synthesized 2D materials belongs to the family of transition metal dichalchogenides (TMDs), which is characterized by a formula unit MX_2, where M is a transition metal and X is usually S, Se or Te. Crystal structure of three-dimensional (3D) TMDs features layers of periodically repeated formula unit, usually in a hexagonal pattern, which are stacked on top of each other and bound together by van der Waals interaction. These layers can be stable when isolated, and their electronic structure can differ significantly from their 3D counterparts, making them prototypical representatives of 2D materials.

Realization of further experimental investigations and practical applications of 2D TMD layers drives a continuous effort in the development of reliable synthesis methods. Recently, a method of obtaining high-quality flakes of a single layer $PtSe_2$ by direct selenization of the Pt(111) surface was presented [2]. Authors of that study have characterized the synthesized layer by x-ray photoelectron spectroscopy, low energy electron diffraction (LEED) scanning transmission electron microscopy (STEM), scanning tunneling microscopy (STM), and angle-resolved photoemission spectroscopy (ARPES), and have further compared the experimental results to the density functional theory (DFT) calculations for a freestanding layer of $PtSe_2$ [2]. The agreement between the theoretical and the experimental results led them to a conclusion that a high-quality monolayer of $PtSe_2$ was successfully synthesized [2].

The hybrid interface between $PtSe_2$ and Pt substrate presented in Ref. [2] could serve as an ideal platform for further chemical functionalization of $PtSe_2$, e.g., in a manner analogous to decoration of MoS_2 on Ir(111) with a Fe cluster [14].

However, the structural and electronic properties of $PtSe_2$/surface hybrid interface are not yet fully understood from the results reported in Ref. [2]. For instance, the distance between the top layer of Pt and $PtSe_2$ is not reported, even though from the distances that were mentioned in the STEM image [2] it can be inferred that it is around 3.3 Å. This observation indicates that the $PtSe_2$ layer is weakly bound on this substrate and therefore physisorbed. Moreover, the results of ARPES are compared only to the band structure of freestanding $PtSe_2$. However, it would be more instructive to compare the ARPES results with the calculation of the band structure of $PtSe_2$ adsorbed on this substrate to validate the proposed $PtSe_2$/Pt(111) structural model in Ref. [2].

Therefore, in this study we present the results of DFT calculations of the geometrical structure, the bonding mechanism, and the band structure of $PtSe_2$ placed onto a clean Pt surface, as was proposed previously [2]. Surprisingly, our results clearly show that $PtSe_2$ is chemisorbed in this case, which is in contradiction with both STEM and ARPES experiments.

Consequently, we propose a different scenario, in which instead of $PtSe_2$ being placed directly onto the clean Pt surface, a monolayer of Se atoms is intercalated between the

*mbosnar@irb.hr
†n.atodiresei@fz-juelich.de

$PtSe_2$ and the surface, passivating the Pt(111) substrate. This scenario is consistent with the STEM image of the system, because in the STEM image Se atoms appear as more diffuse so the passivation layer would correspond to the diffuse layer seen just above the bright dots corresponding to the Pt surface atoms [2]. Also, such intercalation is physically sound, as it could take place during the selenization of the Pt(111) surface. The DFT calculations of bonding energies and ARPES spectra show that in this, Se-passivated, system the $PtSe_2$ monolayer is physisorbed, in agreement with the experiment.

Our results provide an insight into the binding of $PtSe_2$ and the Pt substrate, which is of interest not only as a starting point for further calculations of properties of this system in realistic experimental environments, but also as an example to understand the synthesis of other 2D systems in similar processes.

II. COMPUTATIONAL DETAILS

DFT calculations were performed using the VASP code [16–19], Perdew-Burke-Ernzerhof [20] projected-augmented-wave setups [21] and the optB86b nonlocal van der Waals exchange-correlation functional [22,23]. The plane-wave cutoff was set to 450 eV. Every studied system was relaxed until the force per atom was smaller than 0.01 eV/Å. In relaxations, the Brillouin zone integrals were performed with Methfessel-Paxton smearing of order 1 and the smearing parameter of 30 meV used to treat the electronic occupation numbers. The band structures were calculated with the same smearing, while for the high k-point density calculations to obtain the precise total energies and density of states (DOS), Gaussian smearing of 30 meV was used. All cells involving surfaces contained 15 Å of vacuum along the direction perpendicular to the surface ("z") and dipole correction in that direction was taken into account.

All studied structures were constructed using the theoretically optimized lattice parameters. The optimal lattice parameters for a given system were obtained by fitting the Murnaghan equation of state (EOS) to the DFT energies of that system for its cell volume varying from -3.0% to 3.0% around its experimental value. In the case of Pt, the bulk lattice constant was optimized. For $PtSe_2$ only the a (in-plane) parameter was varied, while c parameter was fixed to be 17.65 Å, and the atoms were allowed to relax. For the calculation of DFT energies to be inserted into the Murnaghan EOS, in the case of the Pt a $21 \times 21 \times 21$ Γ-centered grid was used in the Brillouin zone (BZ) sampling, while for $PtSe_2$ a $15 \times 15 \times 1$ Γ-centered grid was used. The resulting optimal lattice constants are 3.95 Å for Pt and 3.71 Å for $PtSe_2$. Final calculations for $PtSe_2$ with optimized cell parameter were carried out with high density $75 \times 75 \times 1$ BZ sampling, to obtain its total energy and DOS.

To study the adsorption of $PtSe_2$ on the Pt surface, a 4×4 supercell of Pt(111) surface was matched with a 3×3 supercell of $PtSe_2$, as the LEED characterization of the system shows that this configuration occurs in the experiment [2]. The matching, with and without the Se passivation layer, was done using QuantumWise Virtual Nanolab [24]. The optimized-parameter 3×3 supercell of $PtSe_2$ was strained 0.40% to match 4×4 supercell of Pt(111) surface, following an assumption that $PtSe_2$ monolayer would adapt to the bulky surface. The Pt(111) surface was modeled by 5 layers of Pt atoms.

In the case of the passivated surface, we assumed the full coverage of the Pt(111) surface by a monolayer of Se atoms, consistent with the experimental LEED and STEM images [2]. To find the optimal adsorption geometry of Se on Pt, Se

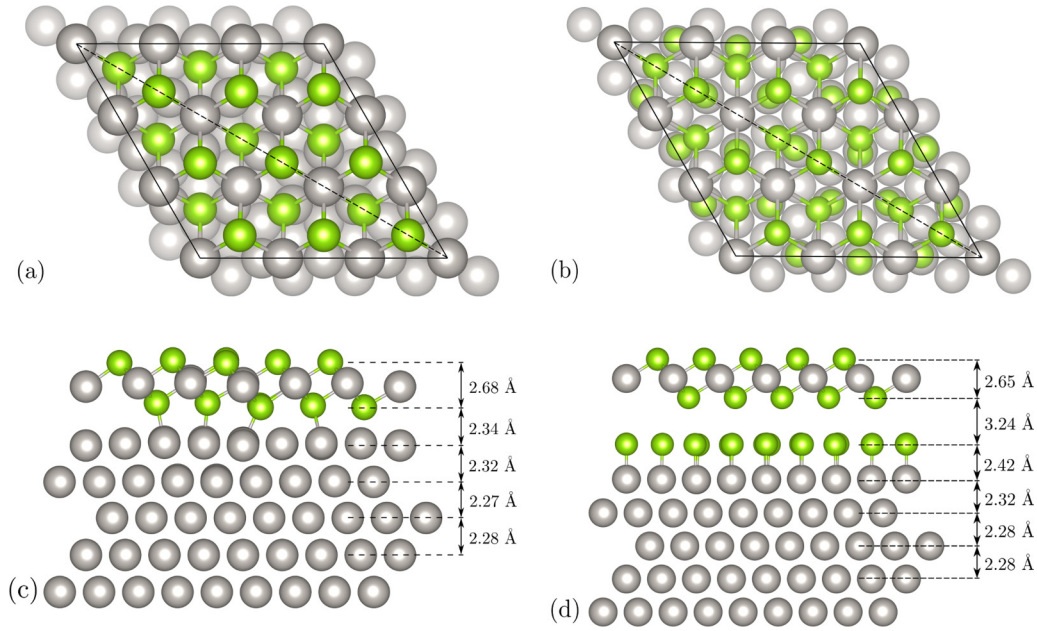

FIG. 1. Top and side view of the optimal energy configurations of $PtSe_2$ on clean [(a) and (c), respectively] and passivated [(b) and (d), respectively] surface. Pt (Se) atoms are drawn in grey (green). Average distances of layers are denoted. The bottom three layers of Pt are equidistant and fixed in relaxation. Figures were made using the VESTA software [15].

adatom was placed on three different sites of a single cell of Pt(111) surface: on-top, hollow and bridge. These configurations were then relaxed, with $20 \times 20 \times 1$ Γ-centered grid being used to sample the BZ and bottom three Pt atoms fixed. Comparison of the obtained energies showed that on-top configuration is optimal [25], which is also consistent with the STEM image.

Two distinct starting coordinations of the surface atoms and $PtSe_2$, constructed using ASE [26], were relaxed to determine the optimal one. Fig. 1 shows the top and side views of the ground-state geometry for both passivated and the clean surface resulting from those calculations. For these relaxations, the BZ was sampled by $5 \times 5 \times 1$ Γ-centered grid and the bottom three layers of Pt were fixed. Finally, to obtain the total energies and DOS for optimized structures of $PtSe_2$ on passivated and clean surface we used a high density $25 \times 25 \times 1$ Γ-centered k-point grid.

To simulate the ARPES image, band structures were calculated for freestanding $PtSe_2$ and $PtSe_2$ on both passivated and clean Pt surface. Since this system features Pt, it is necessary to take the spin-orbit coupling (SOC) into account to reproduce the experimental results. For each structure, a self-consistent calculation was performed with SOC enabled, starting from the electron density obtained from the high k-point density calculations. The BZ for self-consistent SOC calculation was sampled by a $5 \times 5 \times 1$ Γ-centered grid for $PtSe_2$ on the surfaces, and a $15 \times 15 \times 1$ Γ-centered grid for the monolayer $PtSe_2$.

The band structures were calculated for the $K - \Gamma - M - K$ path in the BZ of the $PtSe_2$ unit cell, folded to the BZ of the supercell. The calculations were done with the fixed charge density obtained from the SOC calculations and SOC enabled.

TABLE I. Bonding distances (as defined in text) and bonding energies per Se atom of the $PtSe_2$ layer between surface and the adsorption layer.

System	Bonding distance (Å)	Bonding energy per Se atom (eV)
$PtSe_2$ on clean surface	2.34	1.08
$PtSe_2$ on passivated surface	3.24	0.31
Passivation Se atoms	2.42	1.28

The calculation of the k points of the folded path from the unfolded one, and the unfolding of the spectral density function of the SOC bands projected to the orbitals of $PtSe_2$ from the supercell Brillouin zone to the Brillouin zone of $PtSe_2$ was performed by BandUp code [27,28].

III. RESULTS AND DISCUSSION

The mean vertical distance (i.e., the "bonding distance") between the Se layer of $PtSe_2$ closer to the surface (the bottom layer) and the top Pt layer of clean Pt(111) surface, as shown in Fig. 1(a) and Table I, is approximately 2.34 Å, which suggests chemisorption. On the other hand, the mean vertical distance between the Se layer of passivated surface and the bottom Se layer of $PtSe_2$, shown in Fig. 1(b) and Table I, is approximately 3.24 Å, consistent with the usual physisorption distances. As mentioned in the Introduction, from the distances that are listed on the STEM image in the experimental work [2] it can be estimated that the distance of the diffuse layer above the Pt surface and the bottom Se layer of $PtSe_2$ is approximately 3.3 Å, which is in agreement with our calculation for the Se-passivated surface.

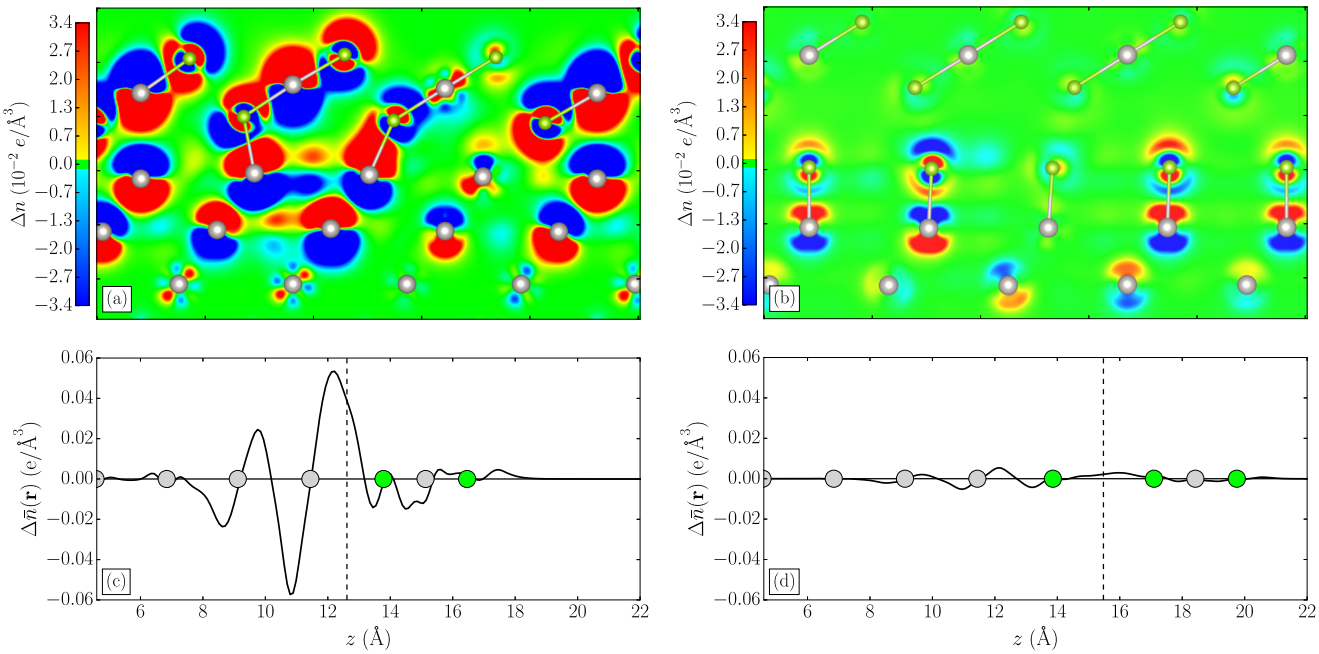

FIG. 2. Upper panels: Electron density difference plots for the case of (a) clean and (b) passivated surface, in a plane denoted by a dashed line in Fig. 1 (upper panels). Lower panels: Plane-averaged electron density difference in the case of (c) clean and (d) passivated surface. Grey (lime) circles denote Pt (Se) atoms. The dashed vertical line denotes the position of midpoint between bottom Se layer of $PtSe_2$ and top layer of the surface. (a) and (b) were made using the VESTA software [15].

Additionally, the distances between the Se layers of $PtSe_2$, and the Pt layers in Pt(111) substrate obtained by the DFT calculations [see Fig. 1(b)] agree reasonably well with the experimentally reported distances in Ref. [2].

The calculated binding energies E_b per bottom Se atom of $PtSe_2$, listed in Table I, are approximately 1.07 eV for $PtSe_2$ on the clean Pt surface and 0.31 eV for $PtSe_2$ on the passivated surface. These energies roughly place adsorption of $PtSe_2$ on clean Pt surface into the regime of weak chemisorption and the adsorption on passivated surface into the regime of physisorption.

For comparison, the adsorption energy of Se atom (singular atoms were deposited onto the surface in the experiment [2]) on Pt surface is $E_b \approx 1.28$ eV per atom, which means that there is greater affinity for formation of the passivating Se layer on the surface than for formation of a $Pt - PtSe_2$ complex on it. Furthermore, this also suggests that the passivation of Pt(111) surface by intercalation of a Se monolayer is preferred to the passivation by formation of a $PtSe_2$ layer directly adsorbed on the surface.

Upper panels in Fig. 2 show a plane cut of the electron density difference between the $PtSe_2$-surface structure and the separate freestanding layer and surface

$$\Delta n(\mathbf{r}) = n_{\text{Surface}|\text{PtSe}_2}(\mathbf{r}) - n_{\text{Surface}}(\mathbf{r}) - n_{\text{PtSe}_2}(\mathbf{r}) \qquad (1)$$

in the case of (a) the clean and (b) the Se-passivated Pt(111) surface. This illustration suggests that the rearrangement of charge at the interface is significantly larger for $PtSe_2$ on the clean surface, and in this case electrons are accumulated at the interface, indicating the formation of chemical bonds between the Se atoms and the atoms of the Pt surface. On the other hand, in the case of $PtSe_2$ on the Se-passivated surface, electron accumulation at the interface is exceedingly small, but there is greater, although still rather small, rearrangement of charge in the TMD layer and the passivated surface. Note that the latter case is similar to the bonding mechanism of graphene on clean and O-intercalated Ir (111) [29,30].

More general analysis of the charge rearrangement can be done by averaging the electron density difference (1) over the $x - y$ plane of the system [31]. This average is shown in panels (c) for clean surface system and (d) for the Se-passivated system of Fig. 2. It confirms that the charge redistribution in adsorption of $PtSe_2$ on clean surface is in general significantly larger compared to adsorption on Se-passivated surface. Specifically, in both systems electrons are accumulated in the interface, but the amount of accumulated electrons in the interface per unit area of the cell, calculated as an integral of the averaged density difference from topmost surface layer to bottom Se layer, is $5.2 \times 10^{-2}\ e/\text{Å}^2$ for clean and $0.5 \times 10^{-2}\ e/\text{Å}^2$ for passivated surface, i.e., an order of magnitude larger. Overall, the charge redistribution suggests chemisorption in the case of clean surface and physisorption in the case of passivated surface.

Following the method of calculating the charge contributing to interface dipole outlined in Ref. [32], we integrate the plane-averaged electron density difference from the selected lower boundary [denoted by a dashed line in Figs. 2(c) and 2(d)] to the point past $PtSe_2$ where it was determined that

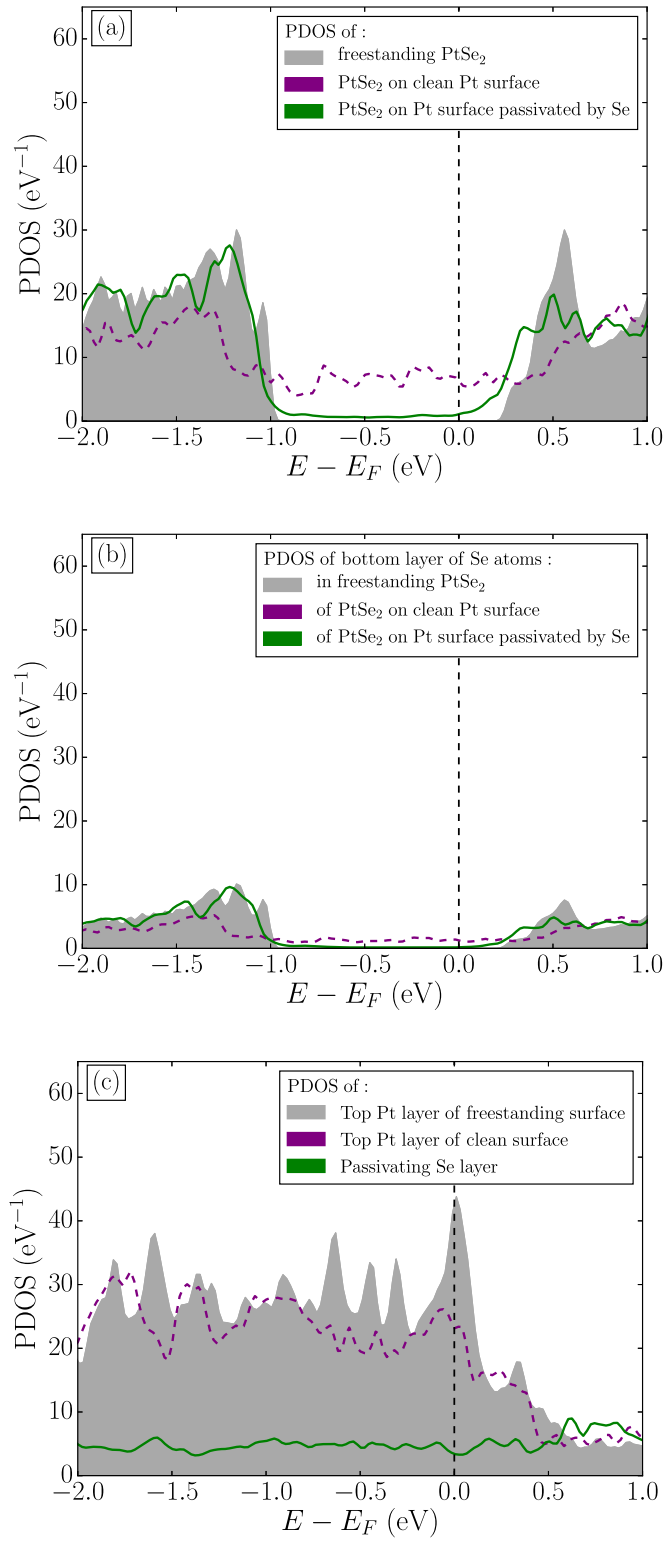

FIG. 3. Projection of DOS on (a) all orbitals of $PtSe_2$ (b) the orbitals of bottom (i. e., closer to the surface) Se layer of $PtSe_2$ and (c) the orbitals of the top layer of the Pt(111) surface near the Fermi level (zero value). In (a) and (b), the PDOS of freestanding $PtSe_2$ and of $PtSe_2$ on clean surface are manually shifted to best fit the PDOS of $PtSe_2$ on surfaces for the sake of simplicity of comparison. The PDOS of freestanding $PtSe_2$ was also multiplied by 9 to match the multiplicity of the supercell.

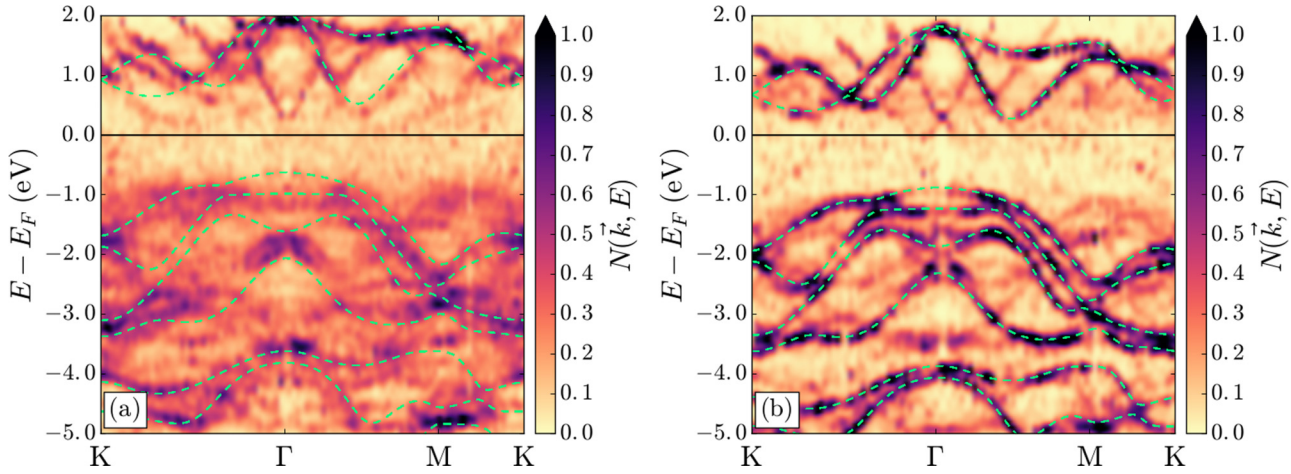

FIG. 4. The unfolded projected spectral density function of $PtSe_2$ on (a) clean and (b) passivated Pt surface. Green dashed lines are the band structure of freestanding $PtSe_2$. The band structure of freestanding $PtSe_2$ has been manually shifted on the energy axis to match the similar features in the unfolded spectral density functions, accounting for the Fermi level shift in adsorption.

the density difference has sufficiently decayed. The lower boundary is set to be at a midpoint of the bottom Se layer and the top layer of the surface, so this integral essentially amounts to amount of electrons redistributed towards $PtSe_2$ in bonding, per area of the supercell. This redistribution is $2.2 \times 10^{-3}\ e/\text{Å}^2$ for $PtSe_2$ on the clean surface and $-1.3 \times 10^{-3}\ e/\text{Å}^2$ for $PtSe_2$ on the passivated surface. Therefore, the charge transfer is small enough to conclude that the electrostatic interactions do not play a role in the bonding mechanism of $PtSe_2$ on either substrate. Consequently, this observation implies that the bonding of $PtSe_2$ on the clean Pt(111) surface is covalent, while it is van der Waals on Se-passivated Pt substrate.

The bonding mechanism can be studied in more detail by analyzing the atom-projected density of states (PDOS). Figure 3(a) shows the comparison of DOS projected on all atomiclike orbitals of $PtSe_2$ adsorbed on both passivated and clean surface, as well as the PDOS of freestanding $PtSe_2$, near the Fermi level. It is clear that the PDOS of freestanding $PtSe_2$ matches that of $PtSe_2$ on the passivated surface, up to small changes due to van der Waals interaction. A significant change occurs with respect to the band gap of the freestanding $PtSe_2$ monolayer, where a small number of states appears, while the conduction band is shifted slightly downwards. The valence band on the other hand loses a peak at -1.0 eV, near the band maximum.

On the other hand, in the case of $PtSe_2$ on the clean surface, there is no resemblance of its PDOS to the freestanding $PtSe_2$ PDOS. Instead of featuring recognizable sharp peaks, the PDOS is smeared out, closing the gap of the frestanding $PtSe_2$. In the same interval of energies, a significant number of Pt states can be found, as shown in Fig. 3(c). Given that the PDOS of Pt surface is also strongly modified between clean and $PtSe_2$ covered surface in the same range of energies, as also seen in Fig. 3(c), it can be concluded that strong hybridization occurs between the lower layer of Se atoms of $PtSe_2$ and Pt atoms on the top layer of the surface.

Another clear demonstration of the difference in the binding of $PtSe_2$ with clean and passivated surfaces is given by the corresponding band structures. Moreover, the calculated band structures can be compared directly to the ARPES measurement, providing a direct link to the experiment. Calculated band structures of $PtSe_2$ on surfaces were unfolded from the supercell to the primitive cell of $PtSe_2$ for sake of comparison with both band structure of freestanding $PtSe_2$ and the ARPES image in [2], as such unfolding is usually performed in processing of experimental data. Figure 4 shows the spectral density functions resulting from unfolding compared to the band structure of the freestanding $PtSe_2$.

The features of the unfolded spectral density function of $PtSe_2$ on the clean surface, shown in Fig. 4(a), especially under the Fermi level, are smeared out and do not match with the band structure of freestanding $PtSe_2$ and the ARPES image. On the other hand, the features of the unfolded spectral density function of $PtSe_2$ adsorbed on the passivated surface, shown in Fig. 4(b), agree well with the bands of freestanding $PtSe_2$ and the ARPES image. Above the Fermi level the matching of the bands of freestanding and adsorbed $PtSe_2$ is good for both the passivated and clean surface, but better for the passivated surface, especially along the $\text{K} - \Gamma$ direction.

A detail shared between the calculated spectral density function of $PtSe_2$ on the passivated surface and the ARPES image is the disappearance of the maximum of the highest occupied band of freestanding $PtSe_2$, around -1.0 eV and the Γ point, and accumulation of the spectral density to region at -1.5 eV both left and right from the Γ point, corresponding to a similar shift in the PDOS. This modification is a consequence of van der Waals interaction between the passivated surface and $PtSe_2$.

IV. CONCLUSIONS

In this theoretical study we investigated the structural and electronic properties of a $PtSe_2$ monolayer on the clean and Se-passivated Pt(111) surface. As a main result, we demonstrated that to reproduce the experimental results, particularly the geometrical structure suggested by STEM and the electronic one by ARPES, the Pt(111) surface must be

Se-passivated such that the $PtSe_2$ monolayer is physisorbed. On the contrary, in the case of the clean Pt(111) surface the $PtSe_2$ layer is chemisorbed and its electronic structure does not resemble the experimental one.

In particular, our DFT calculations indicate that the Pt surface passivation process takes place through the intercalation of Se atoms between the surface and $PtSe_2$, which are chemisorbed on the surface and form a monolayer. This scenario is, on one hand, consistent with the previously obtained STEM image of the system and, on the other hand, consistent with the band structure measured by ARPES. Furthermore, the mean vertical distance between the passivated surface and $PtSe_2$ is 3.24 Å, consistent with usual physisorption distances as well as with the calculated binding energies.

The proposed geometrical model of $PtSe_2$ on Pt(111) can be employed to perform the first-principles calculations of $PtSe_2$ properties in a realistic experimental setup. For instance, one could study activation of $PtSe_2$ for spintronic applications by adsorption of atoms and atomic clusters [33], or by the electrostatic bias, which should induce Rashba splitting [34,35]. These effects could in turn be tested in, e.g., a spin-polarized STM experiment.

ACKNOWLEDGMENTS

M.B. and I.L. acknowledge support from Croatian Science Foundation and the European Union through the European Regional Development Fund within the Competitiveness and Cohesion Operational Programme (Grant No. KK.01.1.1.06) and Center of Excellence for Advanced Materials and Sensing Devices (Grant No. KK.01.1.1.01.0001). V.C., N.A., and S.B. acknowledge support from the Deutsche Forschungsgemeinschaft (DFG, German Research Foundation) - Project No. 277146847 - CRC 1238 (project C01). The authors gratefully acknowledge the Gauss Centre for Supercomputing (GCS) for providing computing time through the John von Neumann Institute for Computing (NIC) on the GCS share of the supercomputer JURECA at Jülich Supercomputing Centre (JSC).

[1] K. S. Novoselov, A. K. Geim, S. V. Morozov, D. Jiang, Y. Zhang, S. V. Dubonos, I. V. Grigorieva, and A. A. Firsov, Electric field effect in atomically thin carbon films, Science **306**, 666 (2004).

[2] Y. Wang, L. Li, W. Yao, S. Song, J. T. Sun, J. Pan, X. Ren, C. Li, E. Okunishi, Y.-Q. Wang *et al.*, Monolayer $PtSe_2$, a new semiconducting transition-metal-dichalcogenide, epitaxially grown by direct selenization of Pt, Nano Lett. **15**, 4013 (2015).

[3] K. F. Mak, C. Lee, J. Hone, J. Shan, and T. F. Heinz, Atomically thin MoS_2: A new direct-gap semiconductor, Phys. Rev. Lett. **105**, 136805 (2010).

[4] B. W. H. Baugher, H. O. H. Churchill, Y. Yang, and P. Jarillo-Herrero, Optoelectronic devices based on electrically tunable p-n diodes in a monolayer dichalcogenide, Nat. Nanotechnol. **9**, 262 (2014).

[5] J. S. Ross, P. Klement, A. M. Jones, N. J. Ghimire, J. Yan, D. G. Mandrus, T. Taniguchi, K. Watanabe, K. Kitamura, W. Yao *et al.*, Electrically tunable excitonic light-emitting diodes based on monolayer WSe_2 p-n junctions, Nat. Nanotechnol. **9**, 268 (2014).

[6] H. Zeng, J. Dai, D. X. Wang Yao, and X. Cui, Valley polarization in MoS_2 monolayers by optical pumping, Nat. Nanotechnol. **7**, 490 (2012).

[7] K. F. Mak, K. He, J. Shan, and T. F. Heinz, Control of valley polarization in monolayer MoS_2 by optical helicity, Nat. Nanotechnol. **7**, 494 (2012).

[8] D. Voiry, A. Goswami, R. Kappera, C. de Carvalho Castro e Silva, D. Kaplan, T. Fujita, M. Chen, T. Asefa, and M. Chhowalla, Covalent functionalization of monolayered transition metal dichalcogenides by phase engineering, Nat. Chem. **7**, 45 (2015).

[9] K. Xu, Z. Wang, F. Wang, Y. Huang, F. Wang, L. Yin, C. Jiang, and J. He, Ultrasensitive phototransistors based on few-layered HfS_2, Adv. Mater. **27**, 7881 (2015).

[10] H. Wang, L. Yu, Y.-H. Lee, Y. Shi, A. Hsu, M. L. Chin, L.-J. Li, M. Dubey, J. Kong, and T. Palacios, Integrated circuits based on bilayer MoS_2 transistors, Nano Lett. **12**, 4674 (2012).

[11] C. Wan, X. Gu, F. Dang, T. Itoh, Y. Wang, H. Sasaki, M. Kondo, K. Koga, K. Yabuki, G. J. Snyder *et al.*, Flexible n-type thermoelectric materials by organic intercalation of layered transition metal dichalcogenide TiS_2, Nat. Mater. **14**, 622 (2015).

[12] B. Radisavljevic, A. Radenovic, J. Brivio, V. Giacometti, and A. Kis, Single-layer MoS_2 transistors, Nat. Nanotechnol. **6**, 147 (2011).

[13] J. Feng, X. Sun, C. Wu, L. Peng, C. Lin, S. Hu, J. Yang, and Y. Xie, Metallic few-layered VS_2 ultrathin nanosheets: High two-dimensional conductivity for in-plane supercapacitors, J. Am. Chem. Soc. **133**, 17832 (2011).

[14] V. Caciuc, N. Atodiresei, and S. Blügel, *Ab initio* study of magnetic nanopatterning of a hybrid transition metal dichalcogenides/Ir(111) system via magnetic clusters, Phys. Rev. Mater. **3**, 094002 (2019).

[15] K. Momma and F. Izumi, *VESTA3* for three-dimensional visualization of crystal, volumetric and morphology data, J. Appl. Crystallogr. **44**, 1272 (2011).

[16] G. Kresse and J. Hafner, *Ab initio* molecular dynamics for liquid metals, Phys. Rev. B **47**, 558 (1993).

[17] G. Kresse and J. Hafner, *Ab initio* molecular-dynamics simulation of the liquid-metal–amorphous-semiconductor transition in germanium, Phys. Rev. B **49**, 14251 (1994).

[18] G. Kresse and J. Furthmüller, Efficiency of *ab initio* total energy calculations for metals and semiconductors using a plane-wave basis set, Comput. Mater. Sci. **6**, 15 (1996).

[19] G. Kresse and J. Furthmüller, Efficient iterative schemes for ab initio total-energy calculations using a plane-wave basis set, Phys. Rev. B **54**, 11169 (1996).

[20] J. P. Perdew, K. Burke, and M. Ernzerhof, Generalized gradient approximation made simple, Phys. Rev. Lett. **77**, 3865 (1996).

[21] G. Kresse and D. Joubert, From ultrasoft pseudopotentials to the projector augmented-wave method, Phys. Rev. B **59**, 1758 (1999).

[22] J. Klimeš, D. R. Bowler, and A. Michaelides, Chemical accuracy for the van der Waals density functional, J. Phys.: Condens. Matter **22**, 022201 (2009).

[23] J. Klimeš, D. R. Bowler, and A. Michaelides, Van der Waals density functionals applied to solids, Phys. Rev. B **83**, 195131 (2011).

[24] D. Stradi, L. Jelver, S. Smidstrup, and K. Stokbro, Method for determining optimal supercell representation of interfaces, J. Phys.: Condens. Matter **29**, 185901 (2017).

[25] The top configuration is 0.49 and 0.47 eV lower from hollow and bridge configurations, respectively.

[26] A. H. Larsen, J. J. Mortensen, J. Blomqvist, I. E. Castelli, R. Christensen, M. Dułak, J. Friis, M. N. Groves, B. Hammer, C. Hargus *et al.*, The atomic simulation environment - a Python library for working with atoms, J. Phys.: Condens. Matter **29**, 273002 (2017).

[27] P. V. C. Medeiros, S. Stafström, and J. Björk, Effects of extrinsic and intrinsic perturbations on the electronic structure of graphene: Retaining an effective primitive cell band structure by band unfolding, Phys. Rev. B **89**, 041407(R) (2014).

[28] P. V. C. Medeiros, S. S. Tsirkin, S. Stafström, and J. Björk, Unfolding spinor wave functions and expectation values of general operators: Introducing the unfolding-density operator, Phys. Rev. B **91**, 041116(R) (2015).

[29] W. Jolie, F. Craes, M. Petrovíc, N. Atodiresei, V. Caciuc, S. Blügel, M. Kralj, T. Michely, and C. Busse, Confinement of Dirac electrons in graphene quantum dots, Phys. Rev. B **89**, 155435 (2014).

[30] C. Busse, P. Lazić, R. Djemour, J. Coraux, T. Gerber, N. Atodiresei, V. Caciuc, R. Brako, A. T. N'Diaye, S. Blügel *et al.*, Graphene on Ir(111): Physisorption with Chemical Modulation, Phys. Rev. Lett. **107**, 036101 (2011).

[31] Here, averaging means that the charge density was integrated over the $x - y$ plane and divided by the surface area of the cell in that plane for each z, hence the unit.

[32] G. Giovannetti, P. A. Khomyakov, G. Brocks, V. M. Karpan, J. van den Brink, and P. J. Kelly, Doping graphene with metal contacts, Phys. Rev. Lett. **101**, 026803 (2008).

[33] Moh. Adhib Ulil Absor, I. Santoso, Harsojo, K. Abraha, H. Kotaka, F. Ishii, and M. Saito, Strong Rashba effect in the localized impurity states of halogen-doped monolayer $ptse_2$, Phys. Rev. B **97**, 205138 (2018).

[34] Q.-F. Yao, J. Cai, W.-Y. Tong, S.-J. Gong, J.-Q. Wang, X. Wan, C.-G. Duan, and J. H. Chu, Manipulation of the large Rashba spin splitting in polar two-dimensional transition-metal dichalcogenides, Phys. Rev. B **95**, 165401 (2017).

[35] A. Manchon, H. C. Koo, J. Nitta, S. Frolov, and R. Duine, New perspectives for Rashba spin–orbit coupling, Nat. Mater. **14**, 871 (2015).